AIP | Applied Physics Letters

# Influence of nanoscale geometry on the dynamics of wicking into a rough surface

Chang Quan Lai, Trong Thi Mai, H. Zheng, P. S. Lee, K. C. Leong et al.

Citation: Appl. Phys. Lett. **102**, 053104 (2013); doi: 10.1063/1.4790183
View online: http://dx.doi.org/10.1063/1.4790183
View Table of Contents: http://apl.aip.org/resource/1/APPLAB/v102/i5
Published by the American Institute of Physics.

# Influence of nanoscale geometry on the dynamics of wicking into a rough surface

Chang Quan Lai,[1,a)] Trong Thi Mai,[2,a)] H. Zheng,[2] P. S. Lee,[3] K. C. Leong,[4] Chengkuo Lee,[2] and W. K. Choi[1,2,b)]
[1]*Advanced Materials for Micro- and Nano-Systems Programme, Singapore-MIT Alliance, Singapore 117576*
[2]*Department of Electrical and Computer Engineering, National University of Singapore, Singapore 117576*
[3]*Department of Mechanical Engineering, National University of Singapore, Singapore 117576*
[4]*GLOBALFOUNDRIES Singapore Pte. Ltd., Singapore 738406*

(Received 22 November 2012; accepted 17 January 2013; published online 4 February 2013)

The dynamics of imbibition into the roughness of a surface was investigated with hexagonal arrays of anisotropic nanofins fabricated with interference lithography and metal assisted chemical etching. It was found that viscous drag caused by the nanofins is similar to that caused by open nano-channels of equal length and height containing the same volume of liquid. In addition, the energy dissipated by form drag for a given driving pressure was determined to be directly proportional to the volume of fluid between nanofin planes that are flat and normal to the imbibition direction. © *2013 American Institute of Physics*. [http://dx.doi.org/10.1063/1.4790183]

Wicking or hemi-wicking, is essentially the imbibition of fluid into the roughness of a surface under the influence of capillary forces,[1] and is an important phenomenon that forms the basis of many natural and engineering applications such as water uptake,[2] moisture management,[3] thermal management,[4] oil recovery,[5] and surface functionalization of microstructures.[6] The process can be observed when a drop of liquid is placed on a rough surface; a thin film of the liquid will seep into the surrounding surface roughness from the base of the droplet, advancing ahead of the droplet and darkening the area it covers.

The velocity of the wicking front is generally accepted to follow a diffusive-like trend such that its displacement increases linearly with respect to the square root of time.[7–9] In the seminal work by Bico *et al.*,[7] it was proposed that this diffusive relationship arises out of a balance between the capillary energy that is providing the pressure to drive the flow and the viscous losses associated with fluid flow past the micro-/nano-structures. Based on this energy balance, Bico *et al.* obtained the displacement-time relationship of the wicking process as[7]

$$z = \left(\frac{2\gamma h}{3\mu\beta}\frac{\cos\theta - \cos\theta_c}{\cos\theta_c}\right)^{\frac{1}{2}} t^{\frac{1}{2}}, \tag{1}$$

where $h$ refers to the height of the micro-/nano-structures, $\theta$ is the contact angle the liquid makes with a flat surface of the substrate material, $\theta_c$ is the critical angle ($0° \le \theta_c \le 90°$), $\gamma$ and $\mu$ are the surface tension and viscosity of the experimenting liquid, respectively.

The role of micro-/nano-structures in retarding the rate of wicking, however, was generalized to an empirically determined coefficient, $\beta$, which represents the drag enhancement factor, i.e., the mean velocity of wicking flow in between micro-/nano-structures is slower than the mean velocity of Poiseuille's flow over a flat plane by a factor of $\beta$.

Previous efforts to shed light on the impedance to wicking flow caused by surface asperities have relied on hydraulic diameter[10] and 2-dimensional approximations[8] and have proven to be difficult without the introduction of fitting parameters or separation of the flow into discontinuous regimes. Our recent work[9] had been able to circumvent such difficulties and provided a more comprehensive analysis of $\beta$ but, like most other studies,[7,8] focused on square arrays of circular nanopillars. Although such symmetrical geometry simplified our analysis, it also restricted the amount of insights that could be gained.

A better approach, therefore, would be to investigate the dynamics of wicking in different directions on a surface decorated with anisotropic micro-/nano-structures. To do so, we make use of interference lithography and metal assisted chemical etching to produce hexagonal arrays of nanofins on flat P-type (100) silicon substrates.[11,12] A total of eleven samples with widely varying dimensions were fabricated for this study.

Figure 1(a) (i)-(iii) show the SEM pictures of some of these nanofins. A schematic diagram and details of the important dimensions of the nanofins are given in Fig. 1(b) and Table I, respectively. Note that Fig. 1(b) also depicts an area $A$ where the mean flow velocity is zero for the case of wicking in $z$ (*normal*) direction—this will be explained in greater detail later. 1 $\mu$l of silicone oil was then deposited at one end of the sample surface and the entire wicking process was recorded at 1000 frames per second using a high speed camera. The experiment was performed in both $z$ (*parallel*) and $z$ (*normal*) directions for each sample. These fabrication and experimental procedures are similar to those used in our previous study.[9]

Figure 2 shows typical $z$ vs. $t^{1/2}$ plots for wicking in the $z$ (*parallel*) and $z$ (*normal*) directions on the same sample. As expected from analysis of Bico *et al.*,[7] the plots exhibit a linear relationship between $z$ and $t^{1/2}$. The linear trend does not extend to the origin, however, which is consistent with the

a)C. Q. Lai and T. T. Mai contributed equally to this work.
b)Author to whom correspondence should be addressed. Electronic mail: elechoi@nus.edu.sg.

 

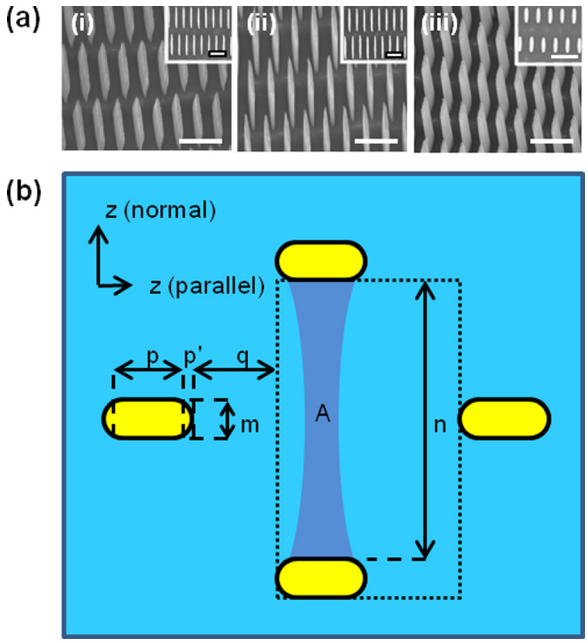


FIG. 1. (a) SEM pictures of Si nanofins of height (i) 1.47 $\mu$m, (ii) 2.63 $\mu$m, and (iii) 3.1 $\mu$m. Top views of the respective nanofins are shown in the insets. All scale bars represent 2 $\mu$m. (b) Schematic diagram of the nanofins. The area of the dark blue region is given by A and the mean velocity of the fluid in this area is assumed to be zero to represent the loss of driving pressure due to form drag when wicking occurs in z (normal) direction. Note also that $p' \ll p$ for all our samples. The dotted line demarcates a unit cell of the nanofin.

results presented in previous studies.[7,9] One of the reasons for this may be due to the influence of droplet spreading during the early stages of wicking. More specifically, when a liquid droplet contacts the nanostructured surface, it can be observed that the droplet rapidly adopts a spherical cap shape on the surface and spreads before the wicking film emerges from the base of the spherical cap. As a result, the dynamics in the initial stages of the wicking process become affected by the inertia of this droplet spreading.

In addition, it is clear that $\beta$, which is inversely proportional to the square of the gradient of the $z$ vs $t^{1/2}$ graphs, is distinctly different for $z$ (*parallel*) and $z$ (*normal*), even when the experiments are conducted on the same sample surface. This implies that nanoscale geometry and the forces retarding the wicking flow, as caused by the nanostructures, are strongly correlated. These retardation forces are essentially viscous drag, which arises due to shear stresses between fluid layers as a result of the "no-slip" condition at the fluid-solid interface, and form drag, which is related to the pressure distribution around the solid body. The magnitude of form drag

TABLE I. Geometrical parameters of nanofins used in this study where $h$ refers to the height of the nanofins, and definitions of $p$, $q$, $m$, and $n$ can be found in Figure 1(b). All dimensions are in $\mu$m.

| | A | B | C | D | E | F | G | H | I | J | K |
|---|---|---|---|---|---|---|---|---|---|---|---|
| ***p*** | 3.00 | 1.47 | 0.95 | 0.74 | 1.17 | 0.74 | 1.12 | 1.21 | 1.13 | 1.00 | 0.85 |
| ***q*** | 0.60 | 0.69 | 1.00 | 0.72 | 0.92 | 1.15 | 1.06 | 1.08 | 1.05 | 0.63 | 0.63 |
| ***m*** | 0.26 | 0.19 | 0.19 | 0.21 | 0.25 | 0.16 | 0.25 | 0.28 | 0.27 | 0.18 | 0.15 |
| ***n*** | 0.67 | 0.81 | 0.64 | 0.55 | 0.57 | 0.58 | 0.71 | 0.69 | 0.64 | 0.31 | 0.32 |
| ***h*** | 2.33 | 1.91 | 2.20 | 1.77 | 3.29 | 3.35 | 3.10 | 2.10 | 1.15 | 2.34 | 1.85 |

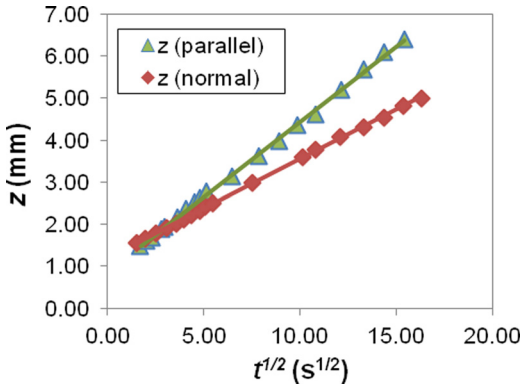


FIG. 2. Representative z vs. $t^{1/2}$ plots obtained experimentally for wicking of silicone oil on a single sample surface. Best fit lines were drawn through the data points.

experienced by a flow is influenced by how streamlined the solid body is.

To establish this correlation theoretically, we first approximate the viscous dissipation associated with a unit cell of the nanofin to be roughly the same as that caused by an open channel of the same height and length (in the direction of the flow) holding the same volume of actively flowing fluid. This approximation has previously been proven to work very well for micro- and nanopillars,[9] giving the expression

$$\beta = \frac{4h^2}{w^2} + 1, \tag{2}$$

where $w$ is the width of the channel which can be easily computed by dividing the volume of actively flowing fluid in a unit cell of nanofin by the height and length of the unit cell.

Next, to account for the energy lost to form drag, we designate a certain volume of fluid in a unit cell of nanofin to be stagnant. In other words, this particular volume of fluid, $V_{form}$, is assumed to have lost all its capillary driving pressure, $\Delta P$, due to form drag and therefore, its mean velocity has fallen from $U_{mean}$ to zero, while the remaining fluid in the unit cell retains $\Delta P$ and continues to flow at $U_{mean}$. The energy loss per unit cell due to form drag caused by a single nanofin, $\Delta E_{form}$,can, therefore, be written as

$$\Delta E_{form} = V_{form}\Delta P. \tag{3}$$

Furthermore, we will assume that $\Delta E_{form}$ is only significant if the nanostructure possesses flat planes that are normal to the capillary flow direction, as such geometry tends to cause the overall structure to be considerably non-streamlined, i.e., there is substantial form drag for wicking in $z$ (*normal*) due to the presence of the plane of area $ph$ but there is no significant form drag for wicking in $z$ (*parallel*) because the rounded ends of the nanofins of length, $p'$, and width, $m$, offer no flat normal planes to impede capillary flow in $z$ (*parallel*). This also implies that $V_{form}$ can only occupy a space within the area $pn$ when wicking takes place in $z$ (*normal*). Therefore, with reference to Fig. 1(b), $V_{form} = Ah = kpnh$, where $0 \le k \le 1$.

The expression for $\beta$ after taking into account both viscous and form drag can then be derived as

$$\beta = \left(\frac{1}{1-f}\right)\left(\frac{4h^2}{w^2} + 1\right), \tag{4}$$

where

$$f = \frac{A}{(1-\phi_s)(p+q)(m+n)}, \tag{5}$$

$$w_p = (1-\phi_s)(m+n), \tag{6}$$

$$w_n = (1-f)(1-\phi_s)(p+q), \tag{7}$$

$\phi_s$ represents the ratio between the area of the top of a nanofin to the area of a unit cell and $f$ represents the fraction of fluid that is stagnant. $w_p$ and $w_n$ represent $w$ calculated for wicking in $z$ (*parallel*) and $z$ (*normal*) directions, respectively.[13] Note that for wicking in $z$ (*parallel*) direction, $f=0$ because of our above assumption that $\Delta E_{form}$, and therefore, $V_{form}$ (from Eq. (3)), is insignificant due to the rounded ends of the nanofins. This applies for circular micro-/nanopillars too, with the consequence that Eq. (4) will be returned to Eq. (2). Thus, it can be seen that the theoretical treatment of $\beta$ presented here is a generalized version that is consistent with the theory presented in our previous study of wicking in circular micro-/nanopillars.[9]

From Eqs. (3)–(7), it can be seen that other than $k$ (embedded in $A$), all of the variables can be determined directly by measuring the dimensions of the nanofins using SEM pictures. To obtain an empirical value of $k$ and investigate how it varies for different samples, we used Eqs. (4) and (5) and experimental values of $\beta$ (*normal*), that is, $\beta$ for wicking in the $z$ (*normal*) direction, to determine $A$ before plotting $A$ against $pn$.

From Fig. 3, it can be seen that $A$ and $pn$ follow a linear relationship and therefore, $k$, which corresponds to the gradient of the plot, is constant for all samples with an approximate value of 0.912. The physical interpretation of this, according to our model, is that 91.2% of the fluid in the area of $pn$ between two consecutive fins has completely lost its driving capillary energy to form drag.

More generally, we can now express $f$ (from Eq. (5)) as

$$f = \frac{0.912pn}{(1-\phi_s)(p+q)(m+n)}. \tag{8}$$

With Eq. (8), $\beta$ in Eq. (4) can now be fully predicted based on the geometry of the nanofins alone.

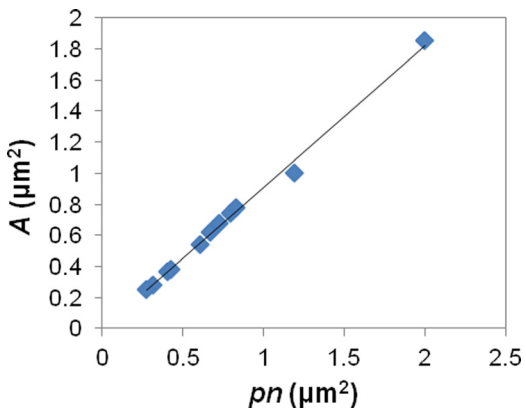


FIG. 3. Plot of A vs. pn. Best fit line is drawn through the data points. Note that the best fit line, which has a gradient value of 0.912, passes through the origin.

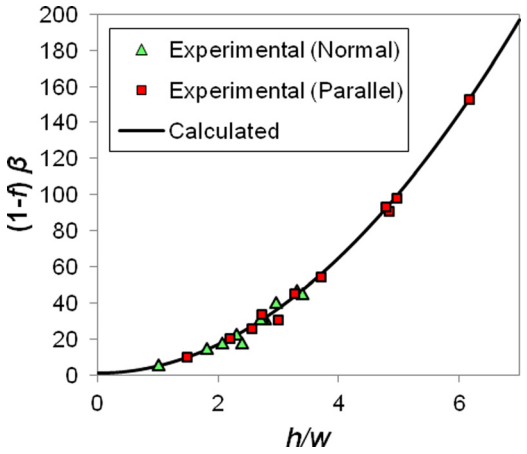


FIG. 4. Experimental values of $(1-f)\,\beta$ vs. h/w. Note that $f=0$ for wicking in z (parallel).

In Fig. 4, the computed values of $\beta$ are validated against experimental results and it can be observed that Eq. (4) provides excellent predictions of $\beta$ in both $z$ (*normal*) and $z$ (*parallel*) directions, indicating that our model accurately reflects the dynamics of wicking in nanostructures.

Other than providing a means of estimating $\beta$ theoretically, Eq. (4) also reveals insights about the wicking process that may not be obvious at first glance. An example of this is the fact that $\beta$ (*parallel*) may not always be necessarily smaller than $\beta$ (*normal*) even though wicking in $z$ (*parallel*) is subjected only to viscous drag whereas wicking velocity in $z$ (*normal*) is retarded by both viscous and form drag. To see how this can be, let us consider the simplified case where $4h^2/w^2 \gg 1$ for wicking in both $z$ (*normal*) and $z$ (*parallel*) directions. It can be easily shown that

$$\frac{\beta(parallel)}{\beta(normal)} = (1-f)\left(\frac{w_n}{w_p}\right)^2. \tag{9}$$

The relationship of $\beta$ (*parallel*) and $\beta$ (*normal*) is, therefore, dependent on the values $f$, $w_n$, and $w_p$, which can combine in the form shown in Eq. (9) to give a value greater than or equal to 1. Plotting the experimental values of $\beta$ (*parallel*)/$\beta$ (*normal*) against $(1-f)(w_n/w_p)^2$ for samples where $h/w > 2$, it can be seen in Figure 5 that Eq. (9) is a valid approximation

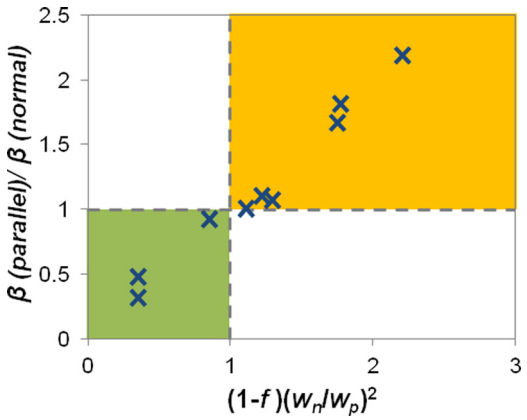


FIG. 5. Plot of $\beta$ (*parallel*)/$\beta$ (*normal*) vs. $(1-f)(w_n/w_p)^2$. $\beta$ (*parallel*) $> \beta$ (*normal*) in the orange region and $\beta$ (*parallel*) $< \beta$ (*normal*) in the smaller green region. No data points were expected to reside in the white regions. Only data from samples with $h/w > 2$ for both $z$ (*normal*) and $z$ (*parallel*) were used in this plot.

for predicting the relative magnitudes of $\beta$ (*parallel*) and $\beta$ (*normal*).

In conclusion, the dependence of wicking dynamics on the geometry of nanoscale surface structures was investigated with ordered arrays of anisotropic nanofins and it was found that nanostructures dissipate flow energy through viscous and form drag. While viscous drag is present for every form of nanostructure geometry, form drag is only associated with nanostructure geometries that have flat planes normal to the wicking direction. It was also discovered that viscous dissipation for a unit cell of nanofin can be effectively approximated with a nano-channel of equivalent height and length that contains the same volume of liquid, while energy dissipation by form drag per unit cell of nanofin is proportional to the volume of the fluid between the flat planes of the nanofins and the driving capillary pressure. With these findings, we are able to establish the dependence of $\beta$, the drag enhancement factor, on the geometrical parameters of the nanostructures. This is important as it provides a precise method for adjusting $\beta$, and therefore wicking velocity, for a given direction on a surface through the selection of appropriate nanostructure geometries.

The authors would like to acknowledge the partial funding of this work by the Singapore-MIT Alliance. C.Q.L., T.T.M., and H.Z. would like to express their deepest gratitude to the Singapore-MIT Alliance, National University of Singapore and GLOBALFOUNDRIES Private Ltd. for provision of research scholarships.

[1]J. Bico, U. Thiele, and D. Quéré, Colloids Surf., A **206**, 41 (2002).
[2]H. Horiguchi, M. Hironaka, V. B. Meyer-Rochow, and T. Hariyama, Biol. Bull. **213**, 196 (2007).
[3]C. R. Buie, J. D. Posnera, T. Fabiana, S.-W. Chaa, D. Kima, F. B. Prinza, J. K. Eatona, and J. G. Santiagoa, J. Power Sources **161**, 191–202 (2006).
[4]C. Zhang and C. H. Hidrovo, in *Proceedings of ASME 2009 Second International Conference on Micro/Nanoscale Heat and Mass Transfer, Shanghai, China, 18-21 December* (2009), pp. 423–437.
[5]X. J. Feng and L. Jiang, Adv. Mater. **18**, 3063–3078 (2006).
[6]M. B. L. Mikkelsen, R. Marie, J. H. Hansen, H. O. Nielsen, and A. Kristensen, Proc. SPIE **8102**, 81020N1–7 (2011).
[7]J. Bico, C. Tordeux, and D. Quéré, Europhys. Lett. **55**, 214–220 (2001).
[8]C. Ishino, M. Reyssat, E. Reyssat, K. Okumura, and D. Quéré, Europhys. Lett. **79**, 56005 (2007).
[9]T. T. Mai, C. Q. Lai, H. Zheng, K. Balasubramanian, K. C. Leong, P. S. Lee, C. Lee, and W. K. Choi, Langmuir **28**, 11465–11471 (2012).
[10]K. M. Hay, M. I. Dragila, and J. Liburdy, J. Colloid Interface Sci. **325**, 472–477 (2008).
[11]W. K. Choi, T. H. Liew, M. K. Dawood, H. I. Smith, C. V. Thompson, and M. H. Hong, Nano Lett. **8**, 3799–3802 (2008).
[12]M. K. Dawood, T. H. Liew, P. Lianto, M. H. Hong, S. Tripathy, J. T. L. Thong, and W. K. Choi, Nanotechnology **21**, 205305 (2010).
[13]See supplementary material at http://dx.doi.org/10.1063/1.4790183 for more details on the experimental procedures and derivations of the various equations.